stellarator news

Published by Fusion Energy Division, Oak Ridge National Laboratory
Building 9201-2 P.O. Box 2009 Oak Ridge, TN 37831-8071, USA

Editor: James A. Rome Issue 67 January 2000
E-Mail: jar@ornl.gov Phone (865) 574-1306 Fax: (865) 574-7624
On the Web at *http://www.ornl.gov/fed/stelnews*

First plasmas in Heliotron J

The Heliotron J Group is very happy to announce that at 7:06 PM on Thursday, 2 December 1999, Heliotron J achieved its first hydrogen discharge by using 1 kW of 2.45-GHz electron cyclotron heating (ECH) at a magnetic field of 500 G, for discharge cleaning. At 3:57 PM on Wednesday, 8 December, Heliotron J achieved its first 53.2-GHz ECH plasma with 300 kW of heating power at a field of 1 T, with an ECH pulse length of about 10 ms. The pulse length is now being increased shot by shot. Figure 1 shows the 53.2-GHz ECH plasma as viewed through one of the tangential ports.

Pictures from the CCD cameras show that the "helical-axis heliotron" plasma is clearly defined by the helical-axis flux surfaces, as expected. For those involved in the years of design, fabrication, and assembly of this new device at Kyoto University, these exciting events signify an important milestone on the way to an optimized helical-axis heliotron. The completed Heliotron J is shown in Fig. 2.

The device parameters are as follows: the plasma major radius is 1.2 m, the average plasma minor radius is 0.1–0.2 m, the magnetic field strength on the magnetic axis is 1–1.5 T, the vacuum rotational transform is 0.3–0.8 with low magnetic shear, and the magnetic well depth is 1.5% at the plasma edge. Heating systems include 0.5-MW ECH, 1.5-MW neutral beam injection (NBI), and 2.5-MW ion cyclotron resonant frequency heating (ICRH).

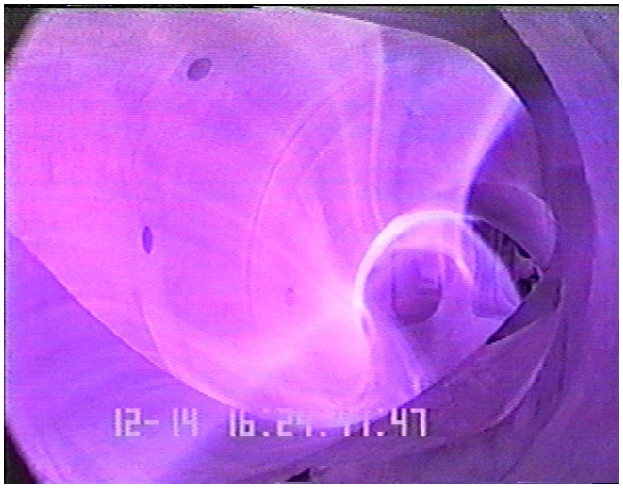

Fig. 1. Photograph of 53.2-GHz ECH plasma in Heliotron J.

T. Obiki, F. Sano, K. Kondo,* M. Wakatani,* T. Mizuuchi, K. Hanatani, Y. Nakamura,* K. Nagasaki, H. Okada, M. Nakasuga,* S. Besshou,* and M. Yokoyama**

E-mail: obiki@ppl.kyoto-u.ac.jp

Institute of Advanced Energy, Kyoto University, Japan
*Graduate School of Energy Science, Kyoto University, Japan
**National Institute for Fusion Science, Toki, Japan

In this issue . . .

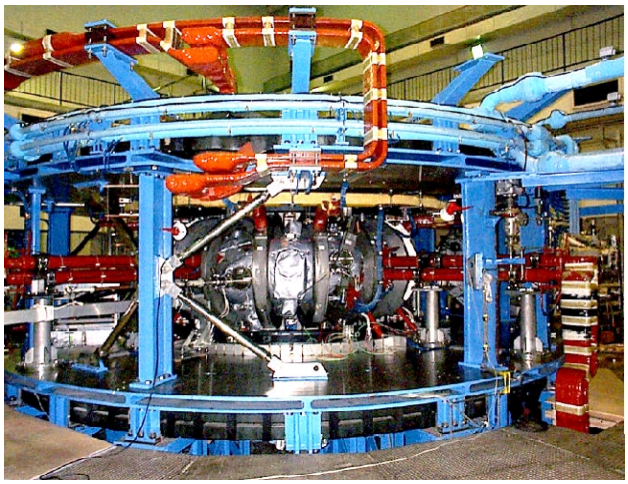

Fig. 2. Photograph of Heliotron J.

Design and experimental program of Heliotron J

The design work for Heliotron J was carried out over a 4-year period, 1995–1999, to develop the successor project to Heliotron E [1]. In order to carry out a new concept exploration experiment in the heliotron line, design efforts were concentrated on mission definition and on the exploitation of operational flexibility by using the existing resources from Heliotron E.

The defined mission of Heliotron J is to add a new chapter to the heliotron series by testing new physics principles that have emerged from recent stellarator theory and by making comparisons with issues previously confronted in Heliotron E, e.g., the high-level compatibility between good particle confinement and MHD stability. The experiments in Heliotron J will allow us to explore the design approach of nonsymmetric, quasi-isodynamic (omnigeneous) optimization in the heliotron line, thus leading to the establishment of design principles for a proof-of-principle (POP) facility based on this concept. Together with these design studies, the physics understanding that is specific to the helical-axis heliotron should be explored to give an integrated picture of the theory and modeling of transport and MHD activity.

Physics design

Helical systems such as heliotrons, which have continuous helical coils, and other advanced stellarators such as W7-AS or HSX, which have modular coils, constitute complementary approaches to stellarator development. Both approaches are needed to develop the physics and engineering understanding of toroidal confinement with special reference to the cost/benefit trade-offs for future coil design. A nonsymmetric, quasi-isodynamic (omnigeneous) optimization of the helical-axis heliotron aims at producing a continuous helical coil design that uses a nonsymmetric magnetic field spectrum to minimize the loss of bounce-averaged drift orbits at high beta. A schematic of Heliotron J is shown in Fig. 1.

The quest to optimize the orbit properties has led us to investigate the improvement in high-energy orbits due to finite beta. In this respect, the bumpiness of the field spectrum was found to be the key component to improving orbit confinement [2]. Minimization of bootstrap current requires both helical and toroidal components. The role of bumpiness as a third parameter should be tested experimentally from the various aspects of its confinement characteristics. The optimal trade-off between a simple coil design, low neoclassical transport, MHD stability, and a practical divertor using the bumpiness parameter remains as an interesting study that challenges us to develop a new concept exploration experiment in the heliotron line.

In contrast to the W7-X design, it is not so easy to access this kind of optimization by using a continuous helical coil system while offering a number of new, interesting physics issues. Our present objective in the design work as well as in the experimental program is to fully develop this design approach based on the concept of a "helical-axis heliotron" and to take a first step toward an optimized helical-axis heliotron.

To minimize cost, a helical-axis heliotron with an aspect ratio $A = 7$ as its standard configuration was selected because it combines the attractive features of good particle confinement and edge magnetic well. The standard configuration can constitute the local isodynamic configuration in the straight confinement section of its $\ell = 1$, $M = 4$ configuration with the helical coil pitch modulation $\alpha = -0.4$ [3].

Extensive collisionless orbit calculations revealed that the prompt orbit loss rate within the vacuum core region was on the order of 20% but could be drastically decreased to 10% with an increase in beta (2%) [4,5]. It was shown that the trapped particles become confined as localized bananas or localized superbananas. The calculations also revealed that even a weak radial plasma electric field (as found in L-mode) can reduce the loss rate to less than 10%. These significant improvements in particle confinement due to beta and radial electric field are expected to introduce a special feature in the experimental confinement of Heliotron J. As an accurate reflection of the particle confinement, the DKES code analysis predicts that the neoclassical ripple transport of Heliotron J is improved with an appropriate choice of bumpiness. As shown in Fig. 4 of Ref. [3], the neoclassical transport coefficient D approaches the same level as that of the equivalent tokamak in the plateau regime when we choose the bumpiness with the opposite sign to the helicity. Furthermore, the

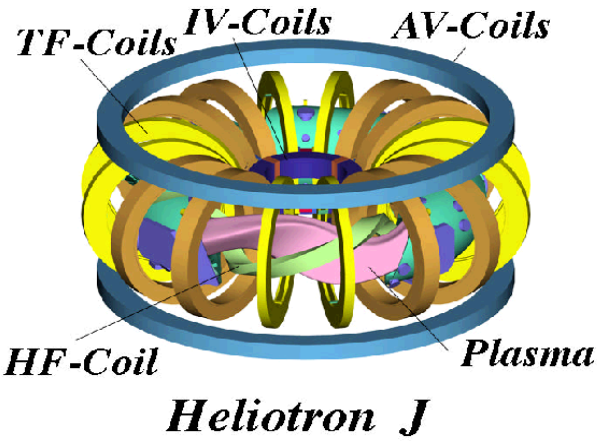

Fig. 1. Schematic of Heliotron J

existence of a weak radial plasma electric field will lead to a major reduction of the 1/ν transport, thus causing it to resemble that of a tokamak. As for the reduction of anomalous transport, the role of $\mathbf{E} \times \mathbf{B}$ plasma flow shear or $\mathbf{E}$ shear can be investigated.

The Heliotron J configuration also presents a number of research topics in MHD equilibrium and stability. The conventional design estimate for the Shafranov shift suggests that the equilibrium beta limit for the standard configuration, β_{eq}, at which the magnetic axis shifts by one-half of the plasma minor radius is on the order of 5%. In the vacuum magnetic configuration, the magnetic well covers the entire volume and is up to 1.5% at the plasma edge, and this well depth increases with an increase in beta. When beta increases, the edge rotational transform in turn decreases, leading to the regime of shear stabilization. The stability beta limit, β_{st}, due to interchange modes is expected to be near 4% from the Mercier criterion. The calculation of the beta limit due to ballooning modes is just beginning, but the result may be much less. It is necessary to carefully study whether the standard ballooning mode analysis provides pessimistic results for the localized modes and to carefully compare those results with the experiment.

The bootstrap current can be balanced to be approximately zero or to be held in a small range by controlling the magnetic field spectrum. In Heliotron J, the helicity produces current with the opposite sign to that arising from the toroidicity. As the third parameter, bumpiness is also expected to control the property of bootstrap current, thus providing additional design freedom for confinement optimization in the helical-axis heliotron line.

The calculation of the Heliotron J edge magnetic field lines shows that two different types of topological structure can serve as a divertor [5]. One is the so-called whisker structure (helical divertor) and the other is the island-chain structure (island divertor). In both cases, the divertor footprints on the wall can be localized (i) in the toroidal direction or (ii) only on the high (or low) field side by adjusting the radial position of the wall. This property would also provide a precious opportunity to investigate the ∇B effects along field lines on the edge plasma transport.

Construction and assembly

The construction of Heliotron J follows the successful experiences with Heliotron E. The key factor was the decision to use a thick vacuum vessel as an accurate guide for the $\ell = 1$ helical coil winding, similar to Heliotron E. Operation with nominal 0.5-s pulsed fields (≤1.5 T) is available while good diagnostic and heating access is maintained. Table 1 shows the project schedule of Heliotron J. Fabrication of the two types of toroidal coils (A and B) started in FY 1996. Toroidal A coils are eight separate coils, 1440 mm in diameter, disposed in the four corner sections of the confinement configuration. Each coil is composed of two sets of 10-turn double pancakes with water-cooled, polyimide/fiber glass-insulated hollow copper conductors (17 mm × 28 mm, 6-mm cooling channel). The maximum current in each conductor is 30 kA, so with four parallel current circuits the total current is 120 kA. The adiabatic temperature rise of the conductor is 55°C with a current density of 68 A/mm^2 in 2.0-s pulsed operation. The toroidal B coils are eight separate coils, 1440 mm in diameter, disposed in the four straight sections. Each coil is composed of a 20-turn double pancake with a water-cooled, polyimide/fiber glass-insulated hollow copper conductor (15 mm × 19 mm, 8.5-mm cooling channel). The maximum current in each conductor is 10.9 kA. The adiabatic temperature rise of the conductor is expected to be 28°C with a current density of 49 A/mm^2 in 2.0-s pulsed operation. Care has been taken to support the mechanical stresses due to the large electromagnetic forces resulting from the combination of toroidal and poloidal fields by using interlocking keys between the coils.

In FY 1997, the circular inner vertical field coil and the two half-torus elements were fabricated. The inner vertical coil is a set of two separate coils, 990 mm in diameter, disposed in the inner side of the torus to control the multipole field components. Each coil is composed of an 80-turn double pancake with an air-cooled, polyimide/fiber glass-insulated copper conductor (6 mm × 50 mm). The maximum current to the conductor is 6 kA. The other poloidal coils necessary for Heliotron J are the outer vertical field coil (AV) and the main vertical coil (V), and for these coils we used existing Heliotron E coils. The half-torus vacuum chamber elements of stainless steel (SUS316) were NC machined to form the precise torus geometry with a helical trough for the helical coil winding. The major radius of the vessel is 1.2 m, and the volume is 2.1 m^3. These half-torus elements were completely welded together at the toroidal

90°–270° plane in compliance with high vacuum requirements. Their D-shaped cross section was determined from the shape of the helical coil and from the requirements of diagnostics and plasma-wall studies. The minimum thickness of the wall is 20 mm. The vessel has 65 ports for pumping, diagnostics, and heating and is positioned and supported against its weight by means of a set of four sliding supports which allow for thermal expansion (2.4 mm in the major radius direction at 100°C) of the vessel during the baking procedure and can withstand earthquakes of 0.3 g. The main pumping for the vacuum vessel is a set of four turbomolecular pumps, each having a pumping speed of 2400 L/s. As a back-up pumping system, a cryopump with a pumping speed of 10,000 L/s for N_2 gas is prepared.

In FY 1998, the highly modulated $\ell = 1$ helical coil parts were fabricated. Each part is composed of eight turns of three parallel conductors (17 mm × 28 mm, 6-mm cooling channel). The maximum current in the conductor is 40 kA with a current density of 90 A/mm^2 (120 kA total). The adiabatic temperature rise of the conductor is 57°C in 1.2-s pulsed operation. In the four toroidal locations, the eight coaxial current feeders of the helical coil current are disposed. An error field with a toroidal mode number of 4 will be inevitable with this arrangement, but its effect on the confinement configuration is calculated to be small.

In FY 1999, final assembly of the fabricated components was carried out. Care was taken in all aspects of the assembly to avoid inaccuracies or perturbations that would create field errors. At each stage of the assembly, detailed measurements of position were made to ensure accuracy. In April, the Heliotron J base and its lower plate were prepared. In May, the two half-torus elements were successfully welded together, preserving the precise torus geometry with an accuracy of 1 mm. After the welding of the torus, in June, the connections of the helical coil parts were made, followed by the installation of the helical coil support. The helical coil support is a toroidally encircling stainless steel plate, 30 mm thick, put on the helical coil to protect against the magnetic hoop forces. In July, the Rogowski coils and diamagnetic loops were arranged in the chamber. In August, the positioning of the vessel and toroidal coils (A and B), the installation of oil piping for the vacuum chamber baking system, the installation of the upper base, and the positioning of the outer vertical coil (AV) were carried out. In September, the coaxial feeders were installed, test pumping of the vessel and relevant leak checks, positioning of the inner vertical coil (IV), and piping for the water cooling were completed. In October, in order to achieve a greater degree of operational flexibility, the power supplies were reorganized. The power source of the old helical plus main vertical coils (H+V) circuit (thyristor bridges) was divided into two blocks, thus providing

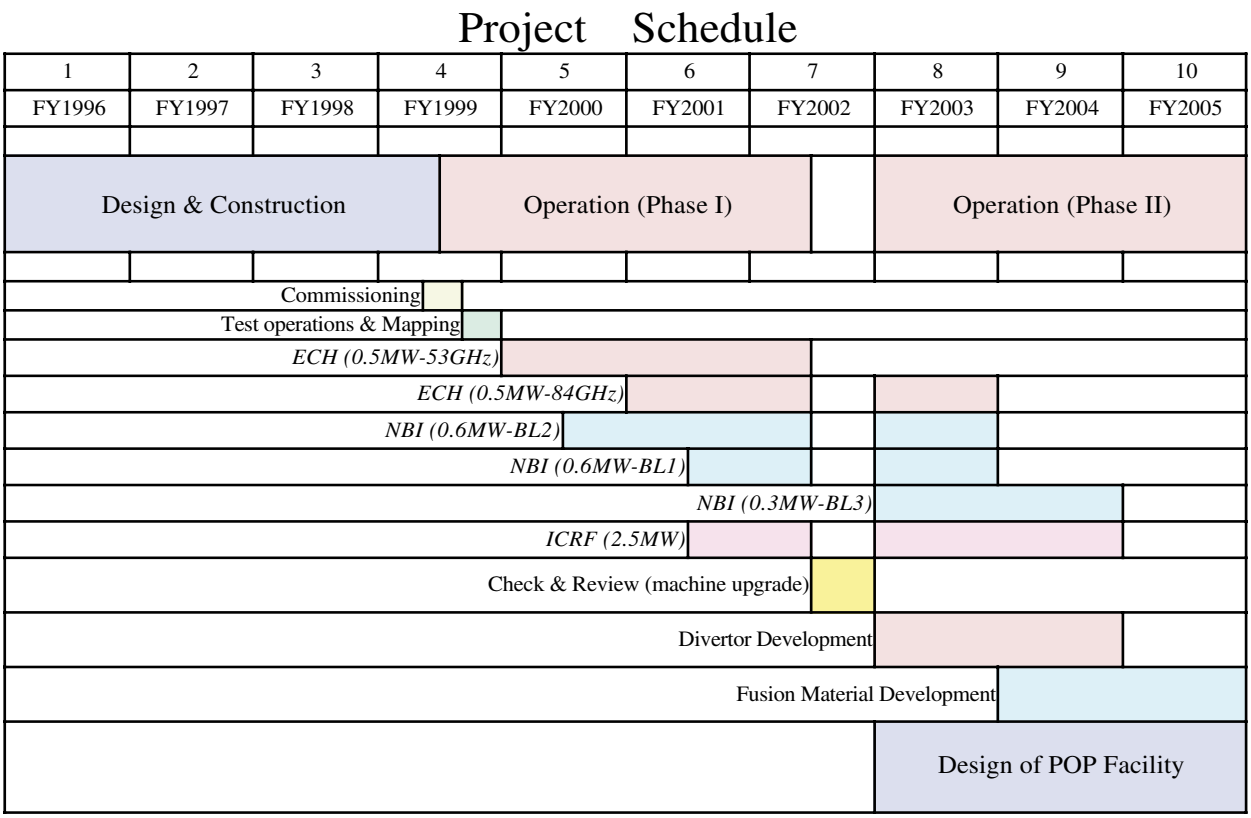

Fig. 2. Heliotron-J project schedule. (FY is April–March.)

a new H+V power source and a new toroidal coils (TA) power source. The relevant busbar and wiring work was also performed.

Experimental Schedule

Developmental operation of Heliotron J will be coordinated through a phased program as shown in Table 1. The key milestones are as follows:

1. Complete the installation of Heliotron J and start the tests and commissioning of the coil system.
2. Review the confinement and stability results for further development of the helical-axis heliotron. The experimental program of Heliotron J is organized to clarify the direction for helical-axis heliotron research beyond the concept exploration level. The key issues are (i) reduced neoclassical transport, (ii) improved beta limit, (iii) compatibility between good particle confinement and MHD with a small bootstrap current, and (iv) exploration of improved confinement modes. The use of separate toroidal coil sets, for example, will provide enough flexibility for experimentally exploring the physics effects of bumpiness. A decision for the device modification or upgrade will depend on the results obtained at this stage.
3. Issue a final design proposal for the next device (the POP facility) during the second operational phase. In order to achieve this, further areas to be investigated are:
   → installation of all the planned additional heating
   → achievement of the ultimate performance of the device
   → installation of a divertor (divertor coil assembly)
   → plasma operation to test and develop materials

The first milestone has been achieved. In order to achieve the second milestone, reliable device operation will be required. Phase I will focus on this goal under constant wall conditions to push the device toward its limits. Experiments in Phase I will provide a good chance for extending heliotron plasma parameters to a new regime and clarifying the keys to improving the confinement. If our approach is successful, then the helical-axis heliotron will offer an attractive and unique option for a future fusion reactor whose configuration properties are under external control for disruption-free, steady-state operation. In Phase II, internal structures will be installed so that a wide range of plasma-wall interaction studies can be made. In this phase, we hope that the successor "POP facility" to meet the third milestone could be designed as the third milestone using optimization principles developed and tested with a divertor.

T. Obiki, F. Sano, K. Kondo,* M. Wakatani,* T. Mizuuchi, K. Hanatani, Y. Nakamura,* K. Nagasaki, H. Okada, M. Nakasuga,* S. Besshou,* and M. Yokoyama**

E-mail: obiki@ppl.kyoto-u.ac.jp

Institute of Advanced Energy, Kyoto University, Japan
*Graduate School of Energy Science, Kyoto University, Japan
**National Institute for Fusion Science, Toki, Japan

References

[1] T. Obiki, T. Mizuuchi, F. Sano, et al., Paper No. IAEA-CN-69/EX2/5 presented at the 17th IAEA Fusion Energy Conference, Yokohama, Japan, 19–24 October 1998.

[2] M. Yokoyama, N. Nakajima, et al., Nucl. Fusion **40** (2), in press (2000).

[3] M. Wakatani, Y. Nakamura, et al., Paper No. IAEA-CN-69/ICP/08(R) presented at the 17th IAEA Fusion Energy Conference, Yokohama, Japan, 19–24 October 1998.

[4] F. Sano, T. Obiki, K. Kondo, et al., presented at the 12th Int. Stellarator Conference, Madison, USA, 27 September–1 October 1999 (to be published in the proceedings).

[5] T. Obiki, F. Sano, M. Wakatani, et al., presented at the 12th Int. Stellarator Conference, Madison, USA, 27 September–1 October 1999 (to be published in the proceedings).

[6] T. Mizuuchi, M. Nakasuga, F. Sano, et al., presented at the 12th Int. Stellarator Conference, Madison, USA, 27 September–1 October 1999 (to be published in the proceedings).

ICRF heating experiment in LHD

Whether ion cyclotron range of frequency (ICRF) heating works as well in helical systems as it does in tokamaks is an important issue. Success in ICRF heating may even be regarded as a cornerstone of the helical concept, for it is directly related to the confinement of high-energy particles. ICRF experiments conducted in CHS and W7-AS have yielded considerable improvement in performance. ICRF experiments in the third campaign of the Large Helical Device (LHD), conducted in fall 1999, were a big step forward.

The preliminary result in the second campaign (1998)

ICRF heating experiments were conducted for the first time on LHD in the second campaign (in 1998). Two water-cooled loop antennas, fed from the top and bottom ports of the LHD device, were used. They are independently movable to maintain an adequate distance from the plasma. For impedance matching, liquid stub tuners were used for the first time in an actual experiment. In these experiments, H_2 was introduced as a minority species in a He plasma.

During this startup phase of LHD, the magnetic field was set to 1.52 T (half of the design value) and the frequency was correspondingly set to 25.6 MHz. The experiment was carried out with a power level of 300 kW. A stored energy increment of 13 kJ was clearly observed, and electron heating was found to be the dominant heating mechanism. There were, however, two problems in the second campaign. One was the modest power attained. It was limited by arcing that occurred in the newly introduced liquid phase shifter. The other problem was an impurity increase during shots, which limited the pulse length to 300 ms.

The experimental result in the third campaign (1999)

ICRF heating was tried again in the third campaign (1999), and drastically improved heating performance was found. The improvement is partly attributed to the increase in the magnetic field, now usually 2.75 T. The frequency was accordingly raised from 26.5 MHz to 38.47 MHz, giving an enhanced loading resistance. The liquid stub tuner was modified from a phase-shifter type to a three-stub type to enhance the overall standoff voltage of the tuner. In order to avoid arcing in the transmission line, a voltage limit of 35 kV was imposed. Thus the utility of the liquid stub tuners for the experiment was demonstrated.

Another factor to be noted is advances in the wall condition. Carbon divertor plates were installed in the third campaign and the metallic impurity influx was drastically reduced. Titanium gettering was also introduced to reduce oxygen. Since a high-density plasma can be sustained by increased ICRF power and reduced impurity concentration, the operational density regime was enlarged in the third campaign. In turn, higher power can be injected at high plasma density because of the increased loading resistance. It is this good sequence of effects that led to the

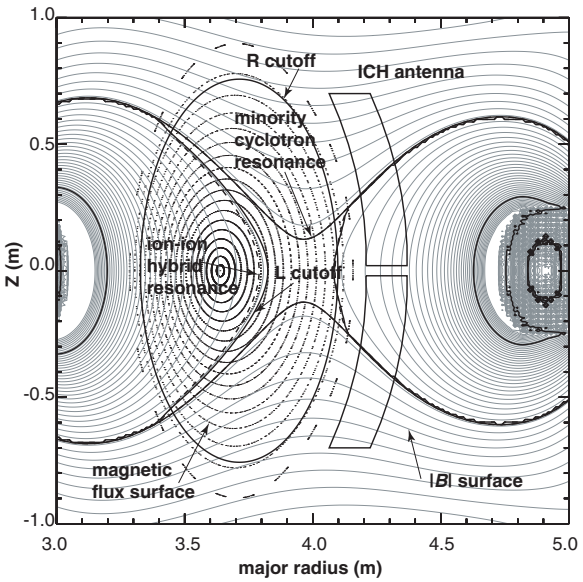

Fig. 1. ICRF heating mode. The locations of the ion cyclotron resonance of the minority ion, the ion-ion hybrid resonance, the R cutoff and the L cutoff are plotted for B = 2.75 T and f = 38.47 MHz.

Magnetic field	1.5 T
Frequency	25.6 MHz
Major radius	3.75 m
Maximum ICRF power	300 kW
Typical plasma density	$\bar{n}_e \approx 0.7 \times 10^{13}\text{cm}^{-3}$
Stored energy increment	$\delta W_p \approx$ 13 kJ

Table 1. Parameters for the second campaign.

Magnetic field	2.75 T
Frequency	38.47 MHz
Major radius	3.6 m
Maximum ICRF power	~1.3 MW
Typical plasma density	$\bar{n}_e \approx (0.5 - 6.0) \times 10^{13}\text{cm}^{-3}$
Stored energy increment	$\delta W_p < 200$ kJ

Table 2. Parameters for the third campaign.

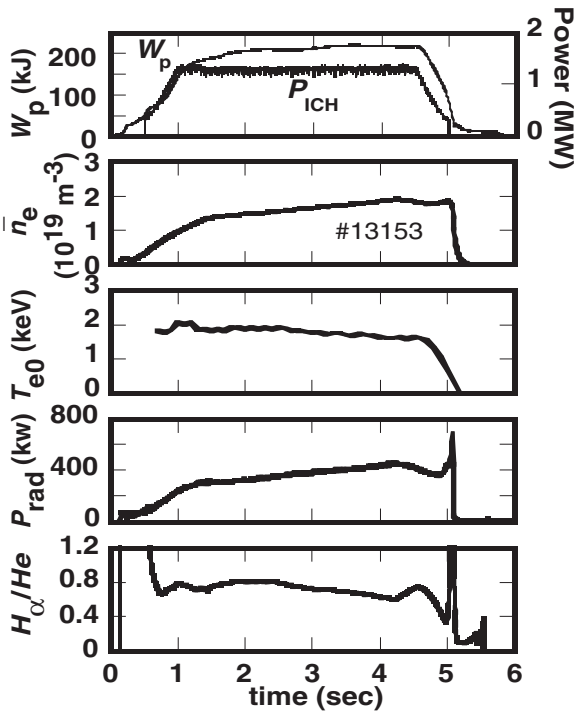

Fig. 2. Time evolution of the parameters of a plasma sustained by ICRF heating alone.

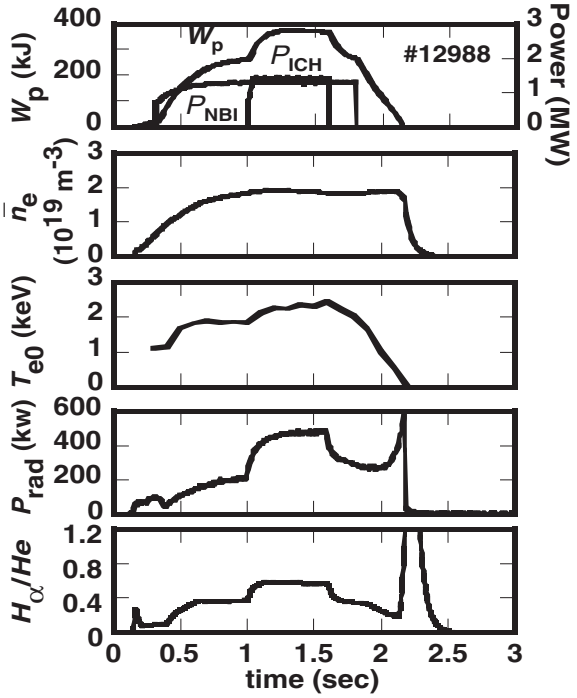

Fig. 3. Time evolution of plasma parameters when ICRF heating is added to an NBI-heated plasma.

remarkable improvement in the performance of the ICRF heating in the third campaign.

Thus, ICRF power of up to 1.3 MW was reliably injected into the plasma allowing for experiments under various conditions; two typical shots are presented in this article. The locations of the cyclotron resonance, cutoff, and mode conversion layers calculated for the experimental parameters are shown in Fig. 1. Proper choice of the heating regime and an inward shift of the major axis may also have played important roles in the improvement of performance.

ICRF self-sustained long-pulse shot

Many previous ICRF heating experiments suffered from a rise in impurities that often led to a thermal collapse of the plasma when the impurity radiation power exceeded the heating power. Therefore, the fact that ICRF heating could sustain the plasma indicates that the impurity problems have been overcome. In the shot shown in Fig. 2, 1.3 MW of ICRF power is injected to sustain the plasma for 5 s following the turning off of the electron cyclotron heating (ECH). The plasma parameters are

$W_p \sim 200$ kJ, $\bar{n_e} \sim 1.8 \times 10^{13}$ cm^{-3}, $T_e \sim T_i \sim 2$ keV.

The radiation power does not increase during the shot as shown in the fourth graph. The bottom graph shows the time behavior of the H_α signal relative to the emission of neutral He indicating that the ratio of hydrogen minority ions to the bulk helium ions does not change.

Once the impurity problem is solved for ICRF heating, it is relatively easy to extend operation to longer pulses. The longest pulse was obtained in the last week of the third campaign, when 0.8 MW of ICRF power sustained a plasma for 68 s with the following parameters:

$W_p \sim 110$ kJ, $\bar{n_e} \sim 1.0 \times 10^{13}$ cm^{-3}, $T_e \sim T_i \sim 2.0$ keV.

Application of ICRF power to an NBI target plasma

ICRF power was applied to a target plasma produced with neutral beam injection (NBI) as shown in Fig. 3. The ICRF power is 1.3 MW and a stored energy increment of 110 kJ was obtained. The stored energy of an NBI + ICRF-heated plasma scales according to ISS95 scaling with a multiplication factor above unity. Thus ICRF and NBI have comparable heating efficiencies. This demonstrates that ICRF can contribute to future high-power experiments as a reliable heating scheme. ICRF heating of the NBI target plasma was observed for the highest plasma densities obtained, 6.0×10^{13} cm^{-3}.

T. Watari for the LHD ICRF Heating Group
National Institute for Fusion Science
322-6 Oroshi-cho, Toki, 509-5292 Japan
Phone: 81-572-58-2212
Fax: 81-572-58-2622
E-mail: watari@nifs.ac.jp